ACS Sustainable Chemistry & Engineering

Research Article

Cite This: ACS Sustainable Chem. Eng. 2019, 7, 6204−6212

pubs.acs.org/journal/ascecg

One-Step Hydrophobic Silica Nanoparticle Synthesis at the Air/Water Interface

Abul Bashar Mohammad Giasuddin, Anthony Cartwright, Kyle Jackson, and David W. Britt*

Department of Biological Engineering, Utah State University, 4105 Old Main Hill, Logan, Utah 84322-4105, United States

Supporting Information

ABSTRACT: A template-free, single-precursor method is presented for constructing hydrophobic silica nanoparticles (NPs) without organic solvent in a Langmuir trough divided into two isolated interfaces connected by a mildly acidic subphase. A water-insoluble trimethoxysilane with an n-propyl side group (nPM) spread at one interface is solubilized upon hydrolysis and diffuses through the subphase to the clean air/water interface where a wire probe tensiometer measures the interfacial sol−gel reaction. Adsorption and assembly of hydrolyzed nPM at the air/water interface is reflected by a steady increase in surface pressure followed by a plateau. Transferred films characterized with FTIR, XRD, SEM, AFM, and water contact angle confirm self-assembly of hydrolyzed nPM into an ∼1 nm thin film at the air/water interface that undergoes polycondensation into sub-10 nm "seed" particles, which further assemble into amorphous, ∼150 nm hydrophobic NPs. Films transferred through the Langmuir−Schaefer method yield modestly hydrophobic surfaces (water contact angles of 115°), whereas aspirated films deposited as a multilayer coating yield superhydrophobic surfaces with contact angles greater than 165°. BET surface area analysis indicates nonporous particles. Longer alkyl-chain organo-silanes (up to C8) also form NPs through this method but with no greater hydrophobicity than the C3 nPM silane. This method provides a facile approach to prepare hydrophobic organo-silane particles using a single short-chain alkyl-silane precursor under purely aqueous conditions.

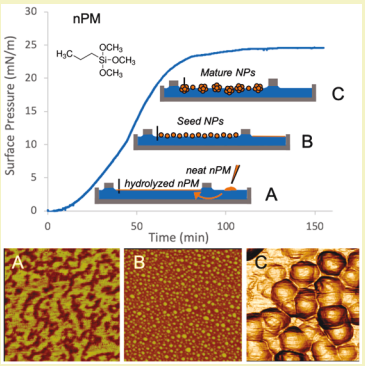

KEYWORDS: *Organo-silane, Silica, n-Propyl-trimethoxysilane, Organically modified silica, Hydrophobic nanoparticle, Self-assembly*

INTRODUCTION

Conventional wet synthesis of hydrophobic silica nanoparticles (NPs) follows a sol−gel process known as the Stöber method,[1] where a silica NP is first synthesized from tetraethylorthosilicate (TEOS) or tetramethylorthosilicate (TMOS) in an alcohol solvent catalyzed with base, followed by purification and isolation steps, then subsequent surface modification.[1−4] This multistep method for synthesizing hydrophobic silica NPs requires an organic solvent such as methanol or ethanol to solubilize the TEOS precursor, followed by base-catalyzed condensation to form NPs that are isolated and purified through centrifugation and washing steps. Exposed silanol (Si−OH) groups on the NP surfaces render the particles hydrophilic and reactive, allowing additional chemistries to be conjugated to the surface, frequently through silanol condensation. Surface hydrophobicity is imparted through a subsequent sol−gel reaction step with an organo- or fluoro-silane designed to form a thin hydrocarbon or fluorocarbon coating, respectively, around the silica NP core. The surface coverage of the hydrophobic capping layer on the NP depends on the core silica NP size, accessible silanols, capping silane properties, and reaction conditions.[2−5] This capping process thus produces waste in terms of a subsequent sol−gel reaction in an organic solvent following the initial sol−gel reaction. It is also inefficient as excess capping agent is required in an effort to form a confluent capping layer on the NPs, which can result in wasted capping material through self-aggregation and sorption on the reaction vessel walls. Depending on conjugation chemistry, a postsynthesis capping step may also lead to entrapment of multiple NPs within a polycondensed capping network.

Coatings of hydrophobic NPs are widely explored for their anticorrosive, low fouling, self-cleaning, antifogging, deicing, and drag reducing properties.[6−19] For most applications of hydrophobic silica NPs, however, the bulk properties (i.e., amorphous SiO_2) are less important than the surface properties and particle size, which dictate the surface energy and topography of thin film coatings prepared from these NPs. Thus, a one-step approach to forming hydrophobic silica NPs using only a single hydrophobic silica precursor is viewed as a more direct and sustainable approach to hydrophobic silica NP synthesis. This also reduces the uncertainty in attaining high surface coverage of the hydrophobic silane capping layer since the capping silane and the core silane are the same, yielding one capping moiety for each silicon atom.

Various hydrophobic TEOS derivatives are commercially available in which one or more of the alkoxy leaving groups has been replaced with an alkyl moiety. In contrast to TEOS,

Received: December 13, 2018
Revised: January 30, 2019
Published: February 13, 2019

DOI: 10.1021/acssuschemeng.8b06359
ACS Sustainable Chem. Eng. 2019, 7, 6204−6212

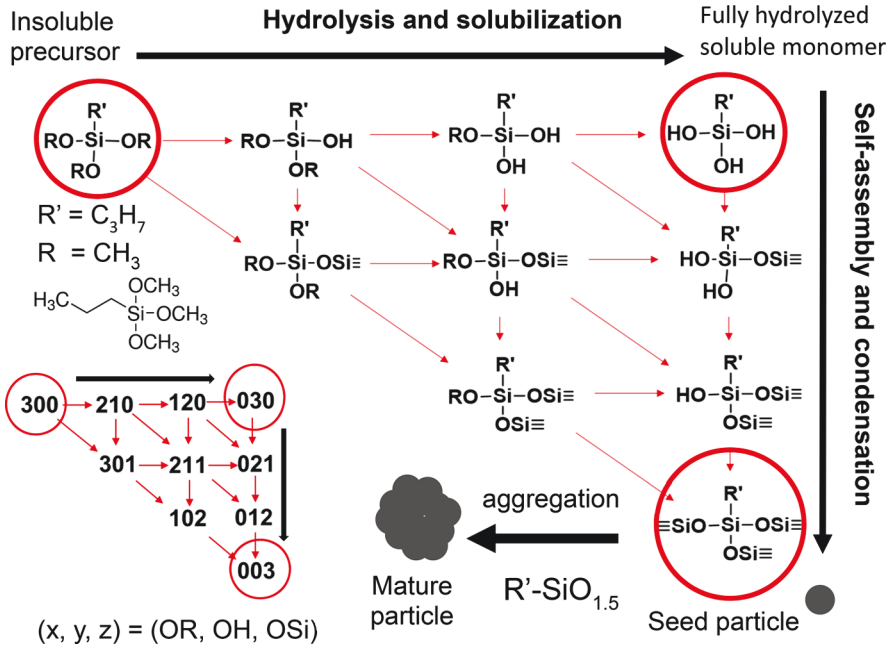

Figure 1. Sol−gel reaction diagram for a monosubstituted organo-silane.

organosilanes (R′-Si-OR_3) exhibit a dipole and are amphiphilic and may thus exhibit self-assembly behavior in aqueous solvent and at the air/water interface, driven by the polarity of the molecule. The propensity for self-assembly through physical interactions (e.g., hydrophobic tail−tail interactions) is accompanied by a reduction in chemical cross-linking, allowing a maximum of three siloxane bonds per silicon atom as shown in the reaction diagram in Figure 1. Multiple silane hydrolysis and condensation paths exist as depicted schematically in Figure 1 for a mono alkyl (R′) trialkoxysilane. In this diagram, an R′-Si-OR_3 precursor is represented numerically as (xyz), where x is the number of −OR substitutions, y the number of −OH substitutions, and z the number of −O−Si substitutions on the silicon atom.[20] Thus, the trialkoxysilane precursor is (300), a silane triol (030), and the fully condensed trisiloxane species (003). As with tetraalkoxysilanes, alkyl-silanes follow distinct pathways depending on whether the reaction is acid or base catalyzed.[21] Basic conditions favor (300) to (003), whereas acidic conditions favor sequential hydrolysis of the (300) precursor to (210), (120), and then (030). The pH of the reaction solution relative to the isoelectric pH (i.e.p.) of the alkyl-silane determines whether an acid, pH < pH(i.e.p.), or base, pH > pH(i.e.p.), reaction mechanism is favored. Solvent and cosolvents influence reaction pathways and final sol−gel products. A low water to silane ratio favors condensation and formation of gels, whereas excess water, especially under acid catalysis, will favor complete hydrolysis followed by polycondensation leading to nanoparticles.

The methoxy groups of an alkyl-silane render it insoluble in water; however, acid-catalyzed hydrolysis yields a fully soluble trisilanol (030) product, increasing the molecule's polarity, amphiphilicity, and propensity for self-assembly to form early condensation products that can further assemble to form small nanoparticle seeds that form mature particles stabilized by intermolecular interactions as indicated in the reaction diagram in Figure 1. The particle surface chemistry is anticipated to be hydrophobic with a stoichiometry of one alkyl group for every Si atom (R′-$SiO_{1.5}$) known as a silsesquioxane, which has chemistry intermediate between a silicone (SiO) and silica (SiO_2). The stoichiometry of one R′ group for each Si is a key benefit of the single precursor synthesis—for a postsynthesis capping, this would correspond to 100% functionalization. If the C−Si bond is highly stable, the R′ to Si ratio will be 1:1 unless the product is calcined. The Si to O ratio may be lower than the optimal 1:1.5 as steric constraints, defects, and reverse reactions (esterification) all contribute to free silanols in the final product. This may be advantageous for nanoparticle assembly as free silanols on early condensation products and seed particles permit covalent intermolecular bonding through silanol condensation.

To investigate hydrophobic NP synthesis from a single organo-silane precursor, we select a monosubstituted short-alkyl chain silane, n-propyl trimethoxysilane (nPM), where the n-propyl side group does not restrict solubility but still imparts hydrophobicity and molecular polarity required for self-assembly. A short R′ chain also presents a lower steric barrier to polycondensation than longer-chain counterparts. nPM is water insoluble due to the hydrophobicity of the three methoxy side groups and the n-propyl chain; however, once hydrolyzed, this three-carbon alkyl-silane is fully water soluble[22] and exhibits amphiphilic behavior with a polar trisilanol headgroup and short alkyl-tail. In contrast, long-chain 18-carbon silanes are water insoluble, even following full hydrolysis, and remain confined to the air/water interface and condense to form two-dimensional organosilane films where in-plane polymerization can be monitored using the Langmuir trough.[23]

In the present work, the Langmuir trough is employed to make a two-compartment reaction system for monitoring nPM hydrolysis, diffusion through the subphase, and self-assembly to form condensed particles. This unique approach to hydrophobic silica NP synthesis requires only a single silane precursor under purely aqueous conditions. Silica NP formation at the air/water interface has been previously explored but required a phospholipid template (DPPC), which was co-spread with TEOS from chloroform on a mildly basic

DOI: 10.1021/acssuschemeng.8b06359
ACS Sustainable Chem. Eng. 2019, 7, 6204−6212

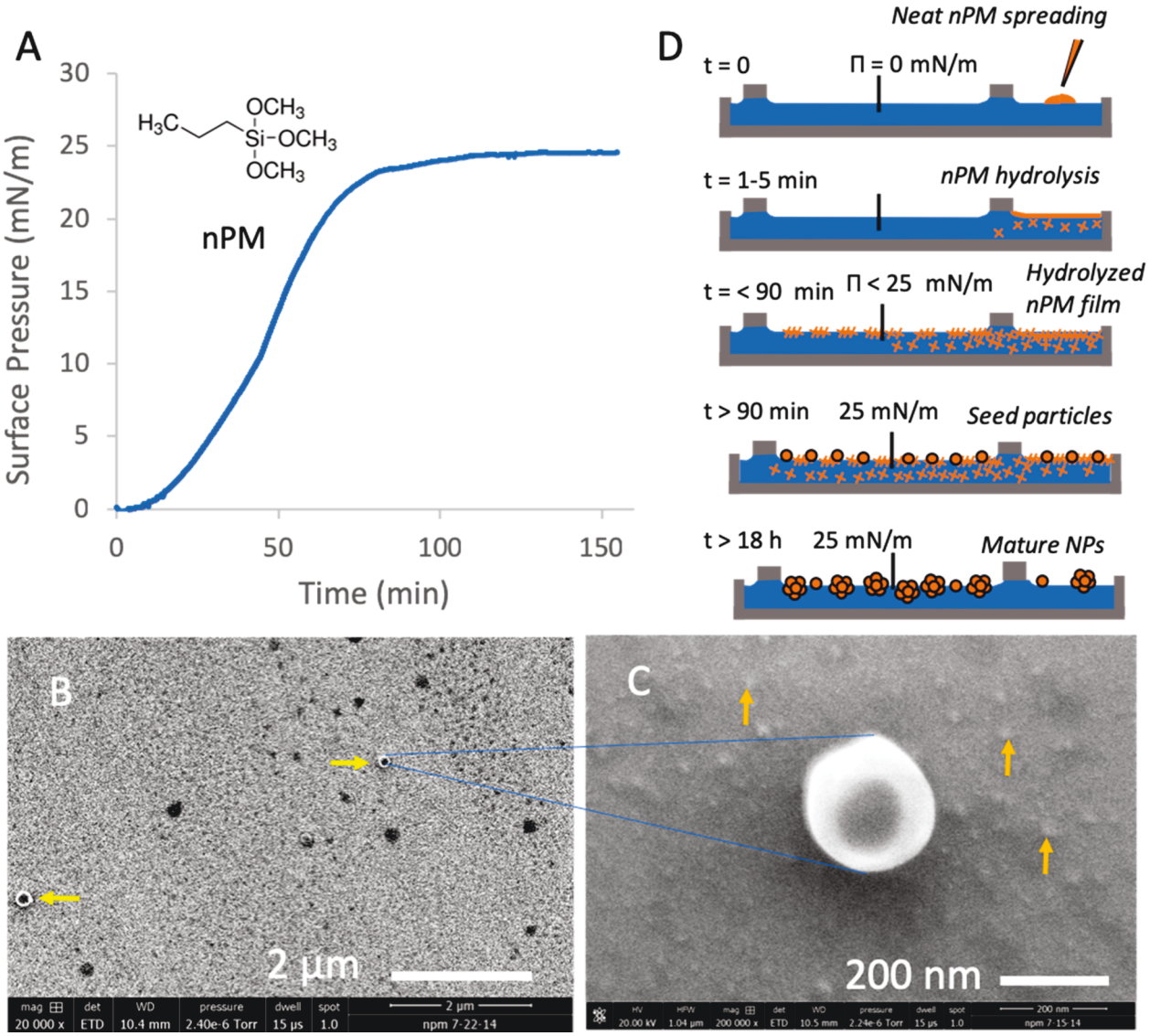

Figure 2. Template-free hydrophobic silica NP formation at the air/water interface using n-propyl-trimethoxysilane (nPM). (A) Kinetics of hydrolyzed nPM self-assembly at the air/water interface monitored through surface pressure increase with time. (B) SEM images of nPM transferred from the air/water interface after 18 h revealing a thin film exhibiting numerous voids or "pinhole" defects. A few spherical nanoparticles (yellow arrows) are observed, and at higher magnification (C) arrays of small nanoparticles are seen to comprise the background (orange arrows). (D) Experimental schematic for spreading neat nPM behind the trough barrier and monitoring hydrolyzed nPM adsorption and assembly into a thin film and NPs at the clean air/water interface.

water surface.[24] This method yielded DPPC-silica composite NPs with sizes ranging between 10−15 nm, depending on DPPC:TEOS stoichiometry; however, in the absence of the templating phospholipid, the TEOS aggregated on the reaction vessel walls and failed to yield NPs.[24] nPM is identical to a TMOS precursor in which a reactive alkoxy group is replaced with an n-propyl side chain, which is demonstrated here to impart amphiphilic behavior that allows for a template-free self-assembly of acid-hydrolyzed nPM into hydrophobic NPs, yielding sub-10 nm seed particles that further assemble into mature ∼150 nm particles. Films transferred through the Langmuir−Schaefer horizontal touch method to glass slides yield modestly hydrophobic surfaces with water contact angles of 115°, whereas superhydrophobic surfaces with contact angles greater than 165° were attained from multilayered NP coatings. Longer alkyl chains, up to eight carbons, are also investigated and observed to yield NPs. For this synthesis method, NPs can be harvested from the air/water interface through dip-coating onto a surface or through vacuum aspiration and drop casting onto a surface. This approach presents an alternative to multistep silica NP synthesis, purification, and capping in organic solvents by demonstrating an aqueous sol−gel synthesis yielding superhydrophobic nanoparticles from a single precursor.

MATERIALS AND METHODS

Source of Chemicals. Double distilled deionized (DDI) water was collected from Barnstead MegaPure Glass Still (Thermo Scientific). The surface tension of the DDI water was measured as 72 mN/m at 21 °C using a Kibron wire probe tensiometer calibrated against HPLC grade water. Dynamic light scattering analysis (Wyatt Nanostar DLS) of the water revealed no scattering. Here, 1.0 N hydrochloric acid (HCl) was purchased from Ricca Chemical Company (Arlington, TX) and diluted to 20 mM, yielding a pH of 2.3. Ammonium hydroxide was purchased from Sigma-Aldrich. n-

DOI: 10.1021/acssuschemeng.8b06359
ACS Sustainable Chem. Eng. 2019, 7, 6204−6212

Propyltrimethoxysilane (nPM, > 95% purity, MW= 164.3, d = 0.94 g/mL) was purchased from Gelest, Inc. (Morrisville, PA). Trimethoxy(octyl)silane (C8-silane, > 96% purity, MW = 234.4, d = 0.91 g/mL) was purchased from Sigma-Aldrich. Hydrophilic fumed silica, Aerosil 200 from Evonik (Parsippany, NJ), was used as received as a control.

Langmuir Trough. Silane hydrolysis, condensation, and nanoparticle assembly were monitored using a glass and PTFE Langmuir trough with a total surface area of 55 cm × 22 cm (Kibron, Inc.) at 21 °C. The subphase was 20 mM HCl (pH 2.3) prepared from DDI water. Silane hydrolysis and condensation were monitored through changes in the surface tension measured using the Kibron wire-probe tensiometer. The probe was prepared by passing through a propane flame followed by DDI rinsing. The trough was kept free of surface-active materials by cleaning with 70% ethanol and then thoroughly rinsing with DDI water. Prior to starting the experiment, the tensiometer was zeroed to measure surface pressure, and the absence of any contaminating surface-active materials was confirmed by compressing the trough barriers without any notable increase in surface pressure above 0.1 mN/m upon full compression. As a further precaution against any surface-active contaminants, the air/water interface on both sides of the trough barrier was vacuum aspirated and the trough covered with a tight-fitting lid, which also reduced evaporation.

At time zero, the tensiometer was set to record surface pressure at 1 s intervals, and a 5 uL drop of neat nPM was spread using a Hamilton gastight syringe at the interface behind the barrier (area set to 10 cm^2) of the Langmuir trough (available area of 112 cm^2). This volume corresponds to 1.708×10^{19} molecules of nPM (calculated from nPM density and molar mass). Assuming a close-packed molecular footprint of nPM is 20 $Å^2$/molecule, then a monolayer of nPM would be composed of 0.5×10^{16} molecules over an area of 10 cm^2. The ratio of $1.708 \times 10^{19}/0.5 \times 10^{16}$ yields 3418 multilayers of close-packed nPM as a feed stock for delivering hydrolyzed nPM to the subphase and central chamber of the trough as depicted in the schematic in Figure 2. Films were transferred from the air/water interfaces either onto an octadecyltrichorosilane (OTS)-modified glass coverslip or freshly cleaved Muskovite mica by a Langmuir–Schaefer (LS) horizontal dip-coat method in which the substrate is placed in contact with the air/water interface and removed. LS transfer was achieved both using a top-down from air into contact with the interface and a bottom-up, where the substrate was immersed in the subphase and brought from below. Aspirating the NPs followed by neutralizing the pH with NH_4OH and drop-casting the freeze-dried powder onto glass or mica substrates yielded multilayered NP films.

SEM. SEM imaging of nPM films transferred by the LS method from the air/water interface to silicon wafers were performed with a FEI Quanta FEG 650 equipped with an Oxford X-Max EDS housed in the Microscopy Core Facility at Utah State University. Samples were imaged between 0.3–0.5 Torr (low vacuum) with 10–14 kV accelerating potential without conductive coatings.

Atomic Force Microscopy (AFM). AFM images of the samples removed by the LS method from the air/water interface were obtained using a Nanoscope III Bioscope (Digital Instrument, Inc.) in tapping mode. Budget Sensors-Tap 300AL-G cantilevers with a tip radius of curvature <10 nm, length 125 μm, width 30 μm, thickness 4 μm and a 40 N/m force constant were employed. Images were collected at 256 × 256 resolution and 1 Hz over a range of scan sizes and scan angles.

Fourier Transformed Infrared Spectroscopy (FTIR). FTIR readings were taken using a Varian 660-IR platform with a horizontal single reflection Pike Technologies MIRacle attenuated total reflectance (ATR) unit, fitted with a ZnSe crystal. After 18 h of nPM reaction time, samples were aspirated from the trough and drop-cast on the ZnSe crystal and air-dried. Resolution Pro Version 5.1.0.822 was used to collect spectra, averaging 20 scans over the range of 600 to 2000 cm^{-1} with a resolution of 1 cm^{-1}. Prior to each reading, a blank background was acquired with the appropriate samples.

Powder X-ray Diffraction (XRD). Aspirated nPM films were freeze-dried, and the powder was manually compacted into XRD metal sample holders to form a smooth, flat surface for analysis. Samples were analyzed using a Panalytical X'Pert Pro X-ray diffraction spectrometer (PW3373/00 Cu LFF DK194241 X-ray) under 45 kV tension and 40 mA current operating conditions. Diffraction patterns were measured from 2θ = 2–75°. The peaks and profiles of the diffraction patterns were interpreted using the X'Pert High Score software program. TEOS SiO_2 NPs formed through traditional Stöber method were analyzed for reference.

Water Contact Angle. The hydrophobicity of the NPs was determined using static water contact angle measurements for the NP films transferred via the LS method from the air/water interface. Layered/close-packed coatings of the NPs were created from NPs by aspirating from the air/water interface followed by freeze-drying to achieve a dry powder that was deposited on double-sided tape on a glass slide. A VCA Optima digital contact angle instrument (AST products, Billerica, MA) was used to measure 6 μL DDI water drops on nPM films transferred using the LS transfer method after 18 h at the air/water interface. Static contact angles were measured for at least 3 drops. The droplets would not release from the needle onto the layered NP coating, and the contact angle was thus measured with the drop adherent to the needle while pressing it into the nPM-coated glass slide. Free droplets were released from a pipet above the surface to demonstrate nonwetting through a high speed video recording of the dynamic droplet (see .mov file in the Supporting Information).

BET Surface Area Analysis. The BET (Brunauer–Emmet–Teller) surface area of the nPM nanoparticles was determined on a MS-16 BET analyzer (Quantachrome Instruments, Boynton Beach, FL, USA). About 0.05 g of dry sample powder was used for measurement. The sample was degassed at 300 °C for 4 h prior to taking triplicate measurements. A standard porous Al_2O_3 sample was analyzed alongside the run to ensure consistency in measurements.

RESULTS AND DISCUSSION

The reaction diagram in Figure 1 depicts the hydrolysis and condensation pathways that a trifunctional silane such as nPM may follow. An acid subphase and excess water to silane were selected here to promote full hydrolysis of the nPM precursor with three methoxy groups, (300), into a trihydrolyzed (030) water-soluble species that freely diffuses through the subphase to the clear air/water interface in the adjacent compartment. Surface assembly of the (030) species is anticipated through its amphiphilic nature, reducing the surface tension at this interface and measured as an increase in surface pressure. Condensation to form silsesquioxane species and seed particles may be promoted at the interface as the interfacial concentration exceeds the bulk silane concentration. Figure 2A shows a surface pressure response following the deposition of neat nPM at the air/water interface behind the barrier on the acidic subphase. The surface pressure measured in the central chamber of the trough remains at zero during nPM spreading, but within 10 min begins to steadily increase as the acid-catalyzed hydrolysis of nPM renders it soluble in the aqueous subphase where it diffuses to the main compartment of the trough and assembles at the air/water interface. Acidic aqueous conditions with excess water favor alkoxy-silane hydrolysis over condensation; thus, it is anticipated that nPM is in a fully hydrolyzed, (030), state prior to the onset of condensation.

Energetic constraints will orient acid-hydrolyzed nPM with the n-propyl "tail" exposed to air and the silanol "head" interfacing with water, forming an amphiphilic thin film that results in the observed surface pressure increase on an acidic subphase. After 90 min, the surface pressure stabilized at ~25 mN/m, suggesting an equilibrium between nPM residing at the

DOI: 10.1021/acssuschemeng.8b06359
ACS Sustainable Chem. Eng. 2019, 7, 6204–6212

interface and nPM in the subphase—this may reflect a completion of hydrolysis and/or uniform distribution of the solubilized nPM throughout the unstirred subphase as well as formation of early condensation products. Under acidic aqueous conditions, Arkles et al. demonstrated nPM sequential hydrolysis and tetramer formation after 90 min using HPLC.[20] Thus, the reaction time observed through surface pressure changes is in general agreement with this study. As hydrolyzed nPM is a water-soluble amphiphile, it is not restricted to the interface and may freely exchange as it forms a Gibbs monolayer, in contrast to a spread Langmuir monolayer comprised of insoluble amphiphiles.[23] The condensation of hydrolyzed nPM could not be discerned from surface pressure measurements, and films were transferred using the LS transfer methods for SEM and AFM analysis.

Low magnification SEM images (Figure 2B) of films transferred after the equilibrium in surface pressure reveals that nPM assembled into a thin film exhibiting defects and a few large (~150−200 nm) spherical particles. At higher magnifications (Figure 2C), numerous small (<10 nm) particles are resolved in the background surrounding the large particles. The smaller particles may serve as nuclei or "seeds" for formation of the larger particles through aggregation and/or addition of additional hydrolyzed nPM. For Gibbs monolayer formation, the air/water interface functions to orient adsorbing hydrolyzed nPM into a film and confines the silanol groups to a plane, which may favor condensation with in-plane neighbors, as well as with hydrolyzed nPM adsorbing to this interfacial film from the subphase. With three reactive groups, trihydrolyzed nPM can condense to form linear (including ladder-like arrangements), cyclic, and network silsesquioxane polymers, which are anticipated to fold into spherical NP geometries to minimize the exposed surface area of hydrophobic nPM side chains to the aqueous solvent. A possible scenario for nPM hydrolysis, diffusion, and assembly into a thin film and self-condensation to form the sub-10 nm seed particles and larger, mature particles is depicted in Figure 2D.

AFM was employed as a complementary imaging modality to SEM to better resolve nPM film phase behavior and to measure the heights of the background particles revealed in Figure 2C. Prior to 90 min, particles are not observed in transferred films; however, AFM reveals that preceding silane assembly into NPs, hydrolyzed nPM self-organizes into a thin film as shown in Figure 3A. Although a three-carbon (C3) alkyl tail is not sufficiently hydrophobic to form a stable and insoluble Langmuir monolayer, evidence of assembly to form domains of uniform ~1 nm tall Gibbs monolayer is seen in Figure 3A. Compression/relaxation cycles of the nPM film (Figure S1, Supporting Information) do not reveal a plateau in surface pressure indicative of a first-order phase transition, which is not unexpected as the short alkyl-tail does not provide a strong stabilizing hydrophobic interaction as observed for long-chain amphiphiles; however, the n-propyl tail provides a sufficient driving force for hydrolyzed nPM adsorption from the subphase and assembly, through physical interactions and chemical condensation, at the air/water interface leading to the surface pressure increase in Figure 2A and the uniform film height in Figure 3A. The trough setup with two chambers is designed such that only hydrolyzed nPM molecules assemble at the clean air/water interface to form a film, which undergoes further restructuring to form isolated domains is seen in Figure 3B; however, unlike Gibbs monolayers composed of longer

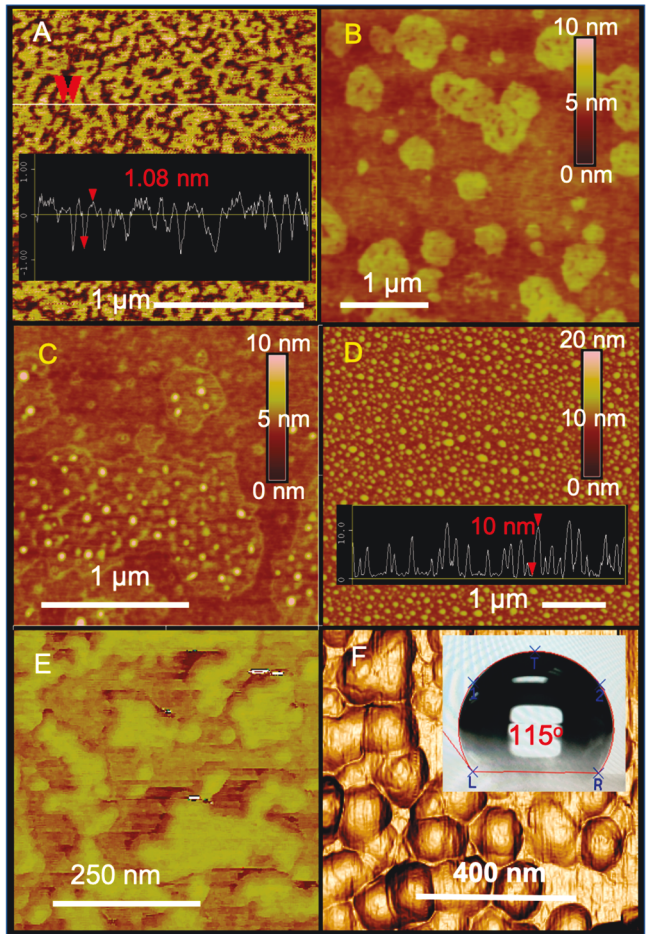

Figure 3. AFM analysis of hydrolyzed nPM self-assembly and condensed NP evolution at the air/water interface (pH 2.3 subphase). (A) nPM thin films (~1 nm height) exhibiting self-assembled domains. (B−C) Nucleation of nPM NPs within the thin film domains. (D) Continued conversion of thin film into NPs yields arrays of sub-10 nm nPM seed particles. (E) In-plane self-association of the seed particles. (F) Continued aggregation to form larger NPs. AFM phase imaging shown in panel E. Derivative of topography shown in panel F for greater edge contrast, with inset showing a static water droplet contact angle.

chain soluble amphiphiles that exhibit rich phase behavior with condensed and highly oriented domains arising from strong hydrophobic interactions among aligned alkyl-tails,[23] domains in the nPM films are less regular. The reactive nature of hydrolyzed nPM, however, provides additional growth and stability, and evidence of nPM condensation within these domains to yield the sub-10 nm NPs seen in SEM imaging (Figure 2) is clearly observed in Figure 3C. This "out-of-plane" growth to form spherical NPs appears to be restricted to the domains, where presumably these seed particles consume the surrounding nPM monolayer. These observations suggest that nPM NPs nucleate and grow through condensation of the surrounding film, thus depleting the film in these domains. Continued conversion of the thin film into sub-10 nm NPs results in arrays of subparticles as observed in Figure 3D. These subparticles appear to further self-aggregate as suggested in Figure 3E, which through continued agglomeration result in the larger "mature" NPs observed Figure 3F. Size histograms for the seed and mature particles are provided in Figure S2 of the Supporting Information.

DOI: 10.1021/acssuschemeng.8b06359
ACS Sustainable Chem. Eng. 2019, 7, 6204−6212

Hydrolyzed NP film assembly may be driven through physical interactions, namely, hydrophobic interactions among the nPM alkyl tails and hydrogen bonding/van der Waals interactions among the silanol heads. The out-of-plane assemblies into sub-10 nm particles observed in Figure 3 could, in theory, be held together through physical forces alone, as is the case for amphiphile assembly into micelles. FTIR analysis of transferred nPM films was employed to determine whether the nPM silane undergoes polycondensation under these experimental conditions. The FTIR spectrum in Figure 4A reveals the expected methylene and methyl bands of the n-propyl chains, which give rise to the C−H stretching at 3000−2850 cm^{-1} (not shown), C−H/C bending at 1420−1100 cm^{-1}, and Si−C vibration at 800 cm^{-1}. The observation of strong Si−O−Si bands between 1210 and 1020 cm^{-1} in the FTIR spectrum confirms that the NPs are polymerized. The absence of an Si−OH band at 950 cm^{-1} that is observed for free silanols[4] further supports polycondensation. A band at 910 cm^{-1} can be discerned, however, which is attributed to free Si−O^- bonds in small silica ring structures.[25,26] These broken or esterified bonds can be attributed to partial cages as depicted in Figure 4B. This may provide insight into the assembly of the early condensation products that assemble into seed particles, which further aggregate into the mature particles. Complete silsesquioxane cage or polyhedron lacks free Si−OH or Si−O^- groups necessary for intermolecular condensation; however, an open cage structure as depicted in Figure 4B, with accessible Si−O^- groups, can undergo interspecies condensation to form Si−O−Si bridges. The intermolecular alignment may be sterically constrained and thus residual Si−O^- is still present in the final NPs as evident by the Si−O^- signal at 910 cm^{-1}.

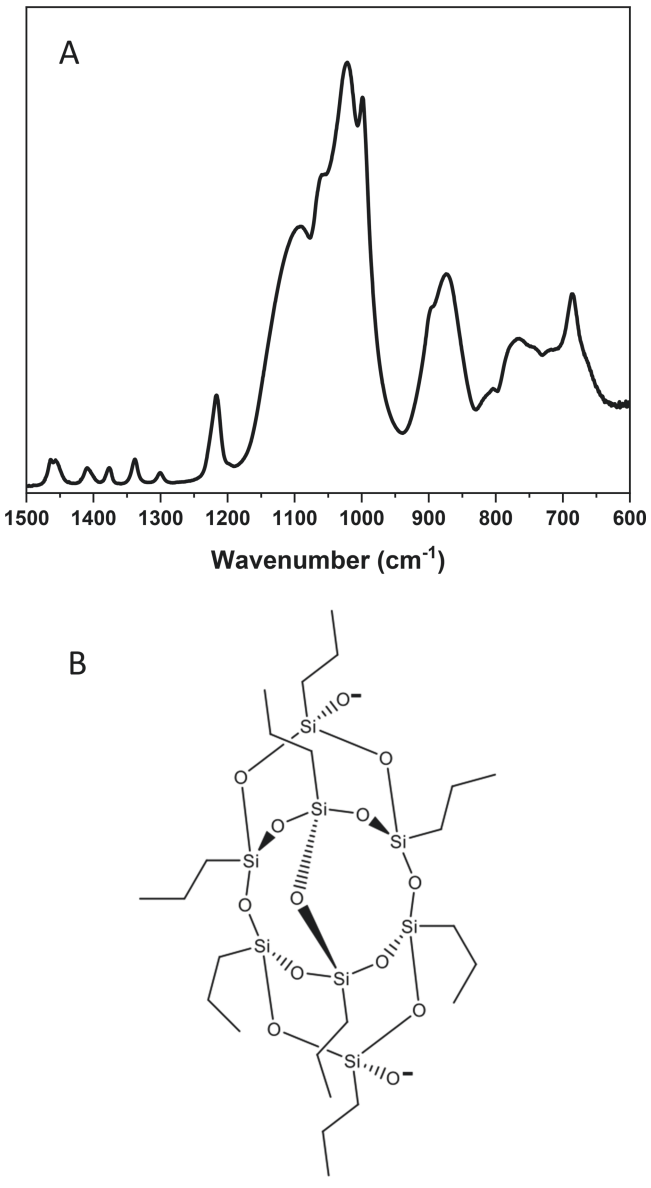

Figure 4. FTIR analysis of nPM NPs. (A) FTIR spectrum confirms nPM polycondensation by strong asymmetric stretching Si−O−Si bands between 1210 and 1020 cm^{-1}. The n-propyl chain gives rise to the C−H stretching at 3000−2850 cm^{-1}, C−H/C bending at 1420−1100 cm^{-1}, and Si−C vibration at 800 cm^{-1}. The band at 910 cm^{-1} is associated with free Si−O^- bonds in small silica ring structures, as depicted in panel B.

While the n-propyl side chain is believed to promote the self-assembly of hydrolyzed nPM into monolayers comprised of domains from which NPs nucleate and grow, it is expected that steric and inductive effects arising from the n-propyl side chains may influence the polycondensation and packing as compared to tetraorthosilicate precursors. Powder X-ray diffraction (XRD) was employed to assess these effects. Figure 5 shows the powder X-ray diffraction patterns for the organo-silica NPs synthesized from nPM, and for reference, that of TEOS-based silica NPs formed through a traditional Stöber method in ethanol/water solvent. NPs synthesized from nPM showed two peaks with 2θ values at 7.4° and 21.2°. These two peaks are attributed to the existence of a ladder-like structure in the macromolecular network, which corresponds to a polyhedral structure as reported for silsesquioxanes in which cross-linking is limited to a maximum of three siloxane bonds per silicon.[27−29] Calculated Bragg d-spacing for the 2θ of 7.4° is 1.2 nm, which represents the interplanar chain to chain distance or the width of each ladder-like double chain.[30] Similarly, the d-spacing for the broad peak of 2θ at 21.2° is around 0.42 nm, which represents the thickness of the ladder-like structure or the spacing between silicon atoms connected

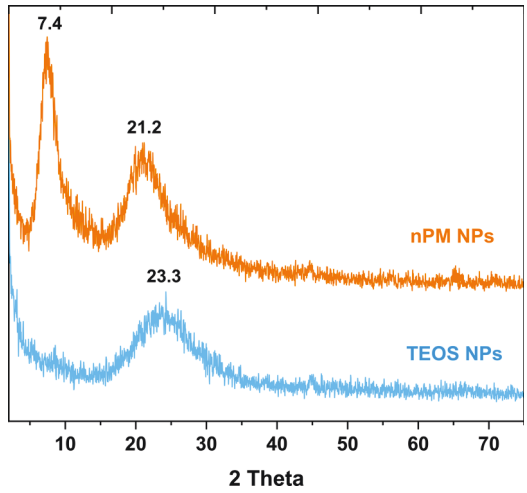

Figure 5. Powder XRD structural analysis of nPM. The X-ray diffraction patterns reveal an amorphous nPM NP structure with bond strain on the Si−O−Si network that is absent for NPs formed from TEOS through the Stöber method. See text for detailed interpretation.

DOI: 10.1021/acssuschemeng.8b06359
ACS Sustainable Chem. Eng. 2019, 7, 6204−6212

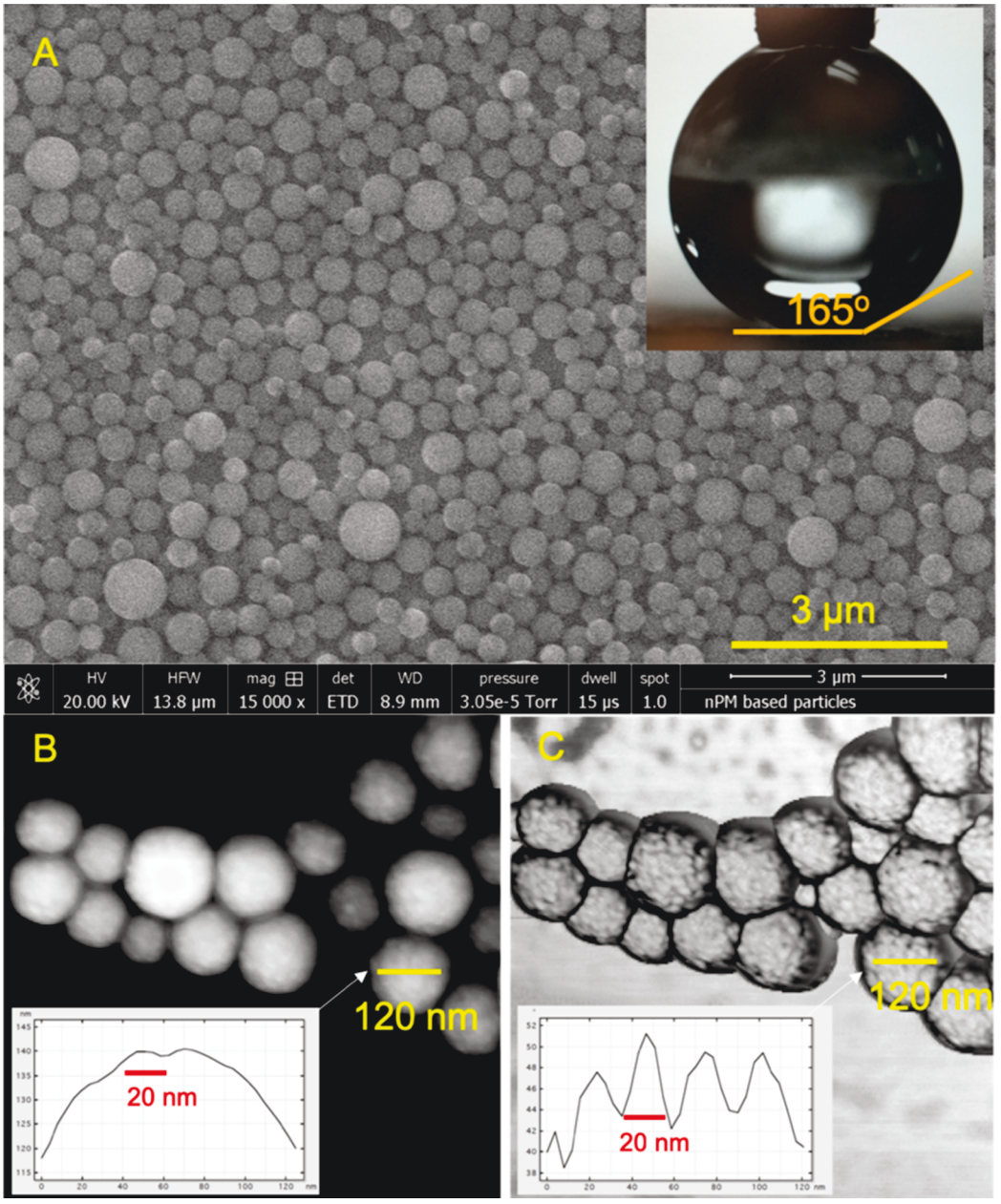

Figure 6. Mature nPM NPs drop-cast following freeze-drying to form a multilayer film (A) exhibiting superhydrophobicity (contact angle in inset and SI video). AFM analysis in topography (B) and phase imaging modes (C) of the NPs following freeze-drying resolve the seed particles from which the mature NPs are comprised. Line profiles (z profiles) across a single mature nPM NP reveal undulations due to the seed particles in both topography (B) and phase (C).

by an oxygen bridge.[31,32] In the X-ray diffraction pattern of the nanoparticles generated from TEOS, only a broad peak of 2θ at 23.3° is observed which is characteristic of amorphous silica.[33,34] The calculated *d*-spacing between silica atoms connected by an oxygen bridge is 0.38 in these nanoparticles which indicates the random nature of intermolecular network. The apparent increased Si−O−Si spacing in the nPM-based nanoparticles (0.42 nm) compared to the TEOS-based nanoparticles (0.38 nm) may arise from an inductive effect of the propyl group in nPM. The polarity of the Si−O bond is somewhat diminished by the n-propyl chain that serves as an electron source to offset the partial positive charge on the silicon atom arising from the pendant electron-withdrawing oxygen groups. This reduction in the Si−O bond polarity thus results in an enhanced bond distance in the Si−O−Si network of the nPM NP.[31] Thus, the n-propyl moiety yields an amorphous silica structure exhibiting backbone bond strain as compared to TEOS-based NPs. X-ray dispersive spectroscopy (EDS) during SEM imaging is presented in the Supporting Information, Figure S3, which within the limits of EDS resolves an approximate $SiO_{1.4}$ structure, close to the anticipated $SiO_{1.5}$ silsesquioxane. EDS of Aerosil 200 fumed silica reports the expected SiO_2 stoichiometry and is provided as reference in Figure S3.

As shown with XRD, the n-propyl moiety influences the assembly and packing of hydrolyzed nPM into a 2-D film at the air/water interface. Out-of-plane growth into the sub-10 nm NPs may be driven by sequestration of the hydrophobic groups to form a hydrophobic core. FTIR demonstrates the presence of the alkyl chains in the resulting NPs; however, the

DOI: 10.1021/acssuschemeng.8b06359
ACS Sustainable Chem. Eng. 2019, 7, 6204−6212

accessibility of the n-propyl chains on the surface of the nPM NPs is unknown and was tested through water contact angle of transferred films. For the LS transfer methods of touching the glass slide to the nPM film at the air/water interface, contact angles of 115° ± 10° (Figure 3F, inset) were attained. This hydrophobicity, although modest, indicates accessibility of the alkyl groups on the NP surfaces. This contact angle for LS-transferred films may also be lower than anticipated due to exposure of the underlying glass substrate, as AFM images (Figure 3) show single layer films with exposed substrate between the NPs. Thus, we explored aspirating the NPs and depositing layered films to prevent contributions from the supporting glass slide. Figure 6A shows an SEM image of this layered film of NPs, which exhibited a contact angle of 165° for a sessile drop that would not release to this surface due to the extreme hydrophobicity. A video of a released droplet bouncing off of this surface illustrates the extreme nonwetting nature and is provided in the Supporting Information. AFM imaging presented in Figure 6B and C of the freeze-dried NPs more clearly resolved the seed particles composing the mature NPs. AFM topography images and line profiles resolved surface undulations in the NPs, which are more distinctly seen to be subparticles in the corresponding phase image and line profile (Figure 6C). The particle growth from subparticle assembly does not appear to create any porosity, as BET surface area analysis of freeze-dried nPM was only 1.9 m^2/g. In contrast, the Aerosil 200 fumed silica has an accessible porosity of 200 m^2/g.

Production of NPs using longer alkyl-chain precursors (C8-trimethoxysilane) was investigated to assess the generality of this method. Following the same protocol employed for the C3 nPM silane, we observed a similar surface pressure kinetic curve, albeit with slower hydrolysis times and a higher final surface pressure (Figure S4). LS transfers revealed formation of both mature NPs and sub-15 nm particles as shown in Figure S5, suggesting formation of seed particles followed by aggregation. Water contact angles for the 8-carbon silane NP film were similar those measured for the nPM particles; thus, no additional benefit was observed for C8 organo-silane over the C3 analog. Additional silane chemistries are being explored with this method of interfacial assembly to generate amorphous silica NPs with surface chemistries defined by the single precursor silane. While the Langmuir trough with tensiometer provides a useful means of measuring reaction kinetics, nPM NPs can be formed in a variety of reaction vessels, such as a Petri dish (Figure S6), that provide a high interfacial area to solution volume. For this one-compartment reaction system, the hydrolyzed silane assembles at the original spreading interface, further simplifying this method of hydrophobic silane assembly and NP formation at the air/water interface.

CONCLUSIONS

In summary, this is a first demonstration of a single precursor, one-step hydrophobic silane synthesis under mildly acidic aqueous conditions. The short alkyl group on nPM imparts hydrophobicity to the resultant NPs without interfering with self-condensation into a network polymer, yielding super-hydrophobic coatings. In contrast to the TEOS-DPPC work of Li et al.,[24] where a phospholipid was required as a template for interfacial assembly, the nPM molecule serves as its own template by nature of its amphiphilicity, forming a thin film that undergoes self-assembly into domains followed by polycondensation into seed particles that appear to further aggregate to yield amorphous, hydrophobic NPs. Increasing the alkyl-tail length of the organo-silane will provide greater self-assembly propensity in forming a Gibbs monolayer, and we demonstrated that octyl-silane forms NPs similar to the n-propyl-silane. Additional hydrophobic surface functionalities such as fluorine may be explored with this method using the respective trifunctional silane precursors that are commercially available, expanding the single precursor approaches to surface-functionalized silica NP formation. A key advantage of the method presented here is the nominally high surface functionality that is obtained when using a single "prefunctionalized" precursor in contrast to postfunctionalization of NPs. With the method developed here, a one to one stoichiometry exists between exposed silicon atoms and the capping moiety that is prebound to each silicon. In addition to being highly efficient in terms of capping, this method reduces waste through eliminating subsequent isolation, washing, and capping steps.

ASSOCIATED CONTENT

Supporting Information

The Supporting Information is available free of charge on the ACS Publications website at DOI: 10.1021/acssuschemeng.8b06359.

Video of water droplet on nPM NP film. (MOV)

nPM compression-relaxation surface pressure isotherms, nPM NP height histograms, SEM-EDS chemical mapping of nPM NP film and fumed silica film, trimethoxy(octyl)silane surface pressure kinetic and AFM images, and AFM image of nPM NPs formed at air/water interface of Petri dish. (PDF)

AUTHOR INFORMATION

Corresponding Author

*E-mail: david.britt@usu.edu. Phone: 1-435-797-2158.

ORCID

David W. Britt: 0000-0002-9753-6404

Notes

The authors declare no competing financial interest.

ACKNOWLEDGMENTS

This research was conducted with funding from the USU AES station, project 1280, AFRI USDA-NIFA 2016-08771, and NSF CBET 1705874 and student support through USU RGS. Assistance with SEM imaging and EDS analysis by Dr. Fen-Ann Shen of the USU Microscopy Core Facility and funding for the SEM instrument through NSF CMMI 1337932 are gratefully acknowledged. BET assistance from Dr. Hossein Jahromi is appreciated.

REFERENCES

(1) Stöber, W.; Fink, A.; Bohn, E. Controlled Growth of Monodisperse Silica Spheres in the Micron Size Range. *J. Colloid Interface Sci.* **1968**, *26* (1), 62−69.

(2) Ren, T.; He, J. Substrate-Versatile Approach to Robust Antireflective and Superhydrophobic Coatings with Excellent Self-Cleaning Property in Varied Environments. *ACS Appl. Mater. Interfaces* **2017**, *9* (39), 34367−34376.

(3) Ye, H.; Zhu, L.; Li, W.; Liu, H.; Chen, H. Constructing Fluorine-Free and Cost-Effective Superhydrophobic Surface with Normal-

DOI: 10.1021/acssuschemeng.8b06359
ACS Sustainable Chem. Eng. 2019, 7, 6204−6212

Alcohol-Modified Hydrophobic SiO_2 nanoparticles. *ACS Appl. Mater. Interfaces* **2017**, *9* (1), 858−867.
(4) Brassard, J. D.; Sarkar, D. K.; Perron, J. Synthesis of Monodisperse Fluorinated Silica Nanoparticles and Their Superhydrophobic Thin Films. *ACS Appl. Mater. Interfaces* **2011**, *3* (9), 3583−3588.
(5) Sriramulu, D.; Reed, E. L.; Annamalai, M.; Venkatesan, T. V.; Valiyaveettil, S. Synthesis and Characterization of Superhydrophobic, Self-Cleaning NIR-Reflective Silica Nanoparticles. *Sci. Rep.* **2016**, *6*, 1−10.
(6) Latthe, S. S.; Terashima, C.; Nakata, K.; Sakai, M.; Fujishima, A. Development of Sol−gel Processed Semi-Transparent and Self-Cleaning Superhydrophobic Coatings. *J. Mater. Chem. A* **2014**, *2* (15), 5548−5553.
(7) Guo, Z.; Guo, F.; Wen, Q.; Peng, Y. Simple One-Pot Approach toward Robust and Boiling-Water Resistant Superhydrophobic Cotton Fabric and the Application in Oil/Water Separation. *J. Mater. Chem. A* **2017**, *5*, 21866−21874.
(8) Zhang, S.; Ouyang, X.; Li, J.; Gao, S.; Han, S.; Liu, L.; Wei, H. Underwater Drag-Reducing Effect of Superhydrophobic Submarine Model. *Langmuir* **2015**, *31* (1), 587−593.
(9) Weng, R.; Zhang, H.; Tuo, Y.; Wang, Y.; Liu, X. Superhydrophobic Drag-Reduction Spherical Bearing Fabricated by Laser Ablation and PEI Regulated ZnO Nanowire Growth. *Sci. Rep.* **2017**, *7* (1), 6061.
(10) Junaidi, M. U. M.; Azaman, S. A. H.; Ahmad, N. N. R.; Leo, C. P.; Lim, G. W.; Chan, D. J. C.; Yee, H. M. Superhydrophobic Coating of Silica with Photoluminescence Properties Synthesized from Rice Husk Ash. *Prog. Org. Coat.* **2017**, *111* (March), 29−37.
(11) Banerjee, I.; Pangule, R. C.; Kane, R. S. Antifouling Coatings: Recent Developments in the Design of Surfaces That Prevent Fouling by Proteins, Bacteria, and Marine Organisms. *Adv. Mater.* **2011**, *23* (6), 690−718.
(12) Syed, J. A.; Tang, S.; Meng, X. Super-Hydrophobic Multilayer Coatings with Layer Number Tuned Swapping in Surface Wettability and Redox Catalytic Anti-Corrosion Application. *Sci. Rep.* **2017**, *7* (1), 1−17.
(13) Wang, N.; Xiong, D.; Deng, Y.; Shi, Y.; Wang, K. Mechanically Robust Superhydrophobic Steel Surface with Anti-Icing, UV-Durability, and Corrosion Resistance Properties. *ACS Appl. Mater. Interfaces* **2015**, *7* (11), 6260−6272.
(14) Wei, Y.; Hongtao, L.; Wei, Z. Preparation of Anti-Corrosion Superhydrophobic Coatings by an Fe-Based Micro/Nano Composite Electro-Brush Plating and Blackening Process. *RSC Adv.* **2015**, *5* (125), 103000−103012.
(15) Shang, Q.; Zhou, Y. Fabrication of Transparent Superhydrophobic Porous Silica Coating for Self-Cleaning and Anti-Fogging. *Ceram. Int.* **2016**, *42* (7), 8706−8712.
(16) Gao, X.; Yan, X.; Yao, X.; Xu, L.; Zhang, K.; Zhang, J.; Yang, B.; Jiang, L. The Dry-Style Antifogging Properties of Mosquito Compound Eyes and Artificial Analogues Prepared by Soft Lithography. *Adv. Mater.* **2007**, *19* (17), 2213−2217.
(17) Cao, L.; Jones, A. K.; Sikka, V. K.; Wu, J.; Gao, D. Anti-Icing Superhydrophobic Coatings. *Langmuir* **2009**, *25* (21), 12444−12448.
(18) Peng, C.; Xing, S.; Yuan, Z.; Xiao, J.; Wang, C.; Zeng, J. Preparation and Anti-Icing of Superhydrophobic PVDF Coating on a Wind Turbine Blade. *Appl. Surf. Sci.* **2012**, *259*, 764−768.
(19) Muginova, S. V.; Myasnikova, D. a; Polyakov, A. E.; Shekhovtsova, T. N. Immobilization of Plant Peroxidases in Cellulose − Ionic Liquid Films. *Mendeleev Commun.* **2013**, *23*, 74−75.
(20) Arkles, B.; Steinmetz, J. R.; Zazyczny, J.; Mehta, P. Factors Contributing to the Stability of Alkoxysilanes in Aqueous Solution. *J. Adhes. Sci. Technol.* **1992**, *6* (1), 193−206.
(21) Kay, B. D.; Assink, R. a. Sol-Gel Kinetics: II. chemical speciation modeling. *J. Non-Cryst. Solids* **1988**, *104* (1), 112−122.
(22) Peng, Y.; Turner, N. W.; Britt, D. W. Trifluorosilane Induced Structural Transitions in Beta-Lactoglobulin in Sol and Gel. *Colloids Surf., B* **2014**, *119*, 6−13.
(23) Britt, D. W.; Hlady, V. Protonation, Hydrolysis, and Condensation of Mono- and Trifunctional Silanes at the Air/Water Interface. *Langmuir* **1999**, *15* (5), 1770−1776.
(24) Li, H.; Pfefferkorn, D.; Binder, W. H.; Kressler, J. Phospholipid Langmuir Film as Template for in Situ Silica Nanoparticle Formation at the Air/Water Interface. *Langmuir* **2009**, *25* (23), 13328−13331.
(25) Chmel, A.; Mazurina, E. K.; Shashkin, V. S. Vibrational Spectra and Deffect Structure of Silica Prepared by Non-Organic Sol-Gel Process. *J. Non-Cryst. Solids* **1990**, *122* (3), 285−290.
(26) Viart, N.; Niznansky, D.; Rehspringer, J. L. Structural Evolution of a Formamide Modified Sol - Spectroscopic Study. *J. Sol-Gel Sci. Technol.* **1997**, *8* (1−3), 183−187.
(27) Lei, X. F.; Qiao, M. T.; Tian, L. D.; Yao, P.; Ma, Y.; Zhang, H. P.; Zhang, Q. Y. Improved Space Survivability of Polyhedral Oligomeric Silsesquioxane (POSS) Polyimides Fabricated via Novel POSS-Diamine. *Corros. Sci.* **2015**, *90*, 223−238.
(28) Liu, C.; Liu, Y.; Shen, Z.; Xie, P.; Zhang, R.; Yang, J.; Bai, F. Study of the Steric Tacticity of Novel Soluble Ladderlike Poly(Phenylsilsesquioxane) Prepared by Stepwise Coupling Polymerization. *Macromol. Chem. Phys.* **2001**, *202* (9), 1581−1585.
(29) Deng, K.; Zhang, T.; Zhang, X.; Zhang, A.; Xie, P.; Zhang, R. A Concerted H-Bonding Self-Assembly-Based Approach to Ladder Poly(Silsesquioxane). *Macromol. Chem. Phys.* **2006**, *207* (4), 404−411.
(30) Rios, X.; Moriones, P.; Echeverría, J. C.; Luquin, A.; Laguna, M.; Garrido, J. J. Ethyl Group as Matrix Modifier and Inducer of Ordered Domains in Hybrid Xerogels Synthesised in Acidic Media Using Ethyltriethoxysilane (ETEOS) and Tetraethoxysilane (TEOS) as Precursors. *Mater. Chem. Phys.* **2013**, *141* (1), 166−174.
(31) Rios, X.; Moriones, P.; Echeverría, J. C.; Luquín, A.; Laguna, M.; Garrido, J. J. Characterisation of Hybrid Xerogels Synthesised in Acid Media Using Methyltriethoxysilane (MTEOS) and Tetraethoxysilane (TEOS) as Precursors. *Adsorption* **2011**, *17* (3), 583−593.
(32) Lana, S.; Seddon, A. X-Ray Diffraction Studies of Sol-Gel Derived ORMOSILs Based on Combinations of Tetramethoxysilane and Trimethoxysilane. *J. Sol-Gel Sci. Technol.* **1998**, *13*, 461−466.
(33) Garcıa-Cerda, L.; Mendoza-González, O.; Pérez-Robles, J.; González-Hernández, J. Structural Characterization and Properties of Colloidal Silica Coatings on Copper Substrates. *Mater. Lett.* **2002**, *56* (4), 450−453.
(34) Kamiya, K.; Dohkai, T.; Wada, M.; Hashimoto, T.; Matsuoka, J.; Nasu, H. X-Ray Diffraction of Silica Gels Made by Sol−gel Method under Different Conditions. *J. Non-Cryst. Solids* **1998**, *240* (1−3), 202−211.

DOI: 10.1021/acssuschemeng.8b06359
ACS Sustainable Chem. Eng. 2019, 7, 6204−6212